# Supporting Information

## Exploratory studies on azido-bridged complexes ($Ni^{2+}$ and $Mn^{2+}$) as dual colourimetric chemosensors for $S^{2-}$ and $Ag^{+}$: combined experimental and theoretical outcomes with real field applications

Nithun Ranjan Pandit,[¥a] Sourav Bej,[¥b,c] Ananya Mondal,[a,d] Meenakshi Ghosh,[d] George E. Kostakis,[e] Annie K. Powell,[f] Priyabrata Banerjee*[b,c] and Biplab Biswas*[a]

[a] *Department of Chemistry, Presidency University, 86/1, College Street, Kolkata 700073, India*
[b] *.Surface Engineering & Tribology Group, CSIR-Central Mechanical Engineering Research Institute, Mahatma Gandhi Avenue, Durgapur 713209, India*
[c] *Academy of Scientific & Innovative Research (AcSIR), AcSIR Headquarters CSIR-HRDC Campus, Postal Staff College Area, Sector 19, Kamla Nehru Nagar, Ghaziabad – 201002, Uttar Pradesh, India*
[d] *Vidyasagar College for Women, 39 Sankar Ghosh Lane, Kolkata, 6, West Bengal, India*
[e] *School of Life Sciences, University of Sussex, Falmer, BN1 9QG, United Kingdom*
[f] *InstitutfürAnorganischeChemie, Karlsruhe Institute of Technology (KIT), Engesserstr. 15, D-76131 Karlsruhe, Germany.*

† Footnotes relating to the title and/or authors should appear here

Electronic Supplementary Information (ESI) available: [details of any supplementary information available should be included here]. See DOI: 10.1039/x0xx00000x

¥Equal Contribution

| Sl. No. | Description | Entry |
|---|---|---|
| 1 | Different coordination modes of azide co-ligand | Scheme S1 |
| 2 | Thermo Gravimetric Analysis | Fig. S1 |
| 3 | Different orientational view of BS-1 | Fig. S2 |
| 4 | Selected bond lengths and bond angles of BS-1 | Table S1 |
| 5 | Different orientational view of BS-2 | Fig. S3 |
| 6 | Sulphide mediated reduction scheme of azide centre | Scheme S2 |
| 7 | Selected bond lengths and bond angles of BS-2 | Table S2 |
| 8 | B-H plot of BS-1 with $S^{2-}$ | Fig. S4 |
| 9 | Limit of detection of BS-1 for $S^{2-}$ | Fig. S5 |
| 10 | B-H plot of BS-1 with $Ag^{+}$ | Fig. S6 |
| 11 | Limit of detection of BS-1 for $Ag^{+}$ | Fig. S7 |
| 12 | Comparative study of BS-1 with different anions | Fig. S8 |
| 13 | Comparative study of BS-1 with different cations | Fig. S9 |
| 14 | Effect of pH | Fig. S10 |
| 15 | B-H plot of BS-2 with $Ag^{+}$ | Fig. S11 |
| 16 | Limit of detection of BS-2 for $Ag^{+}$ | Fig. S12 |
| 17 | Comparative study of BS-2 with different cations | Fig. S13 |
| 18 | Time-dependent response of BS-1 & BS-2 towards targeted analytes | Fig. S14 |
| 19 | FT-IR of BS-1 with $S^{2-}$ and $Ag^{+}$ | Fig. S15a & Fig. S15b |
| 20 | FT-IR of BS-2 with $Ag^{+}$ | Fig. S16 |
| 21 | ESI-MS of BS-1 with $S^{2-}$through intermediate | Fig. S17 |
| 22 | Geometry optimised structure of BS-2 with their HOMO-LUMO energy gap | Fig. S18 |
| 23 | ESI-MS of BS-1 monomeric unit with $S^{2-}$ | Fig. S19 |
| 24 | ESI-MS of BS-1 with $Ag^{+}$ | Fig. S20 |
| 25 | ESI-MS of BS-2 with $Ag^{+}$ | Fig. S21 |

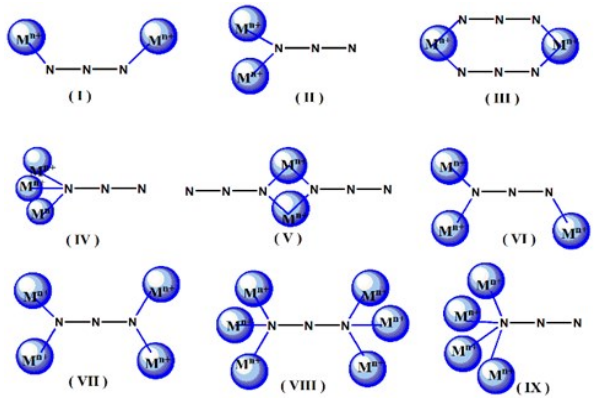


**Scheme S1** Different coordination modes of azide co-ligand

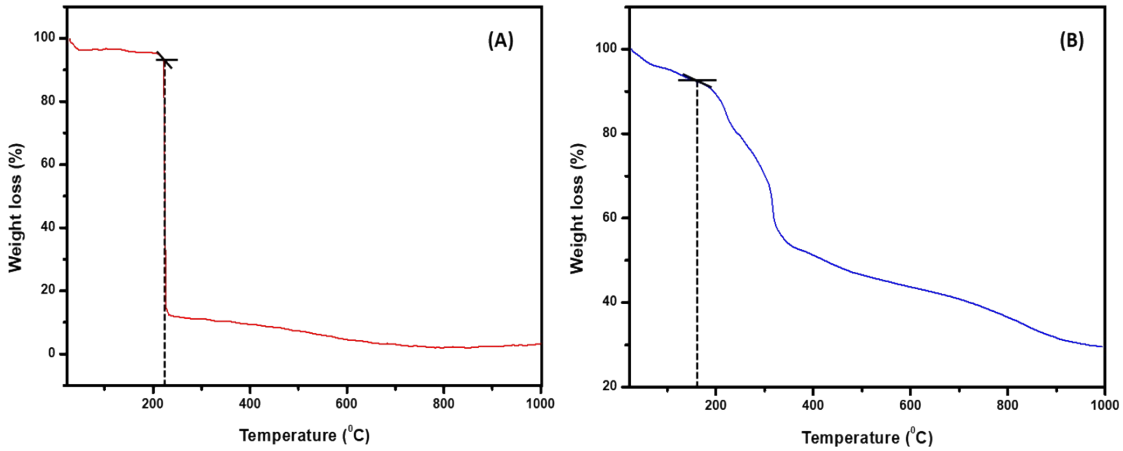


**Fig. S1** Thermo Gravimetric Analysis of (A) BS-1 (B) BS-2 showing the stability of 225 $^0$C and 190 $^0$C respectively

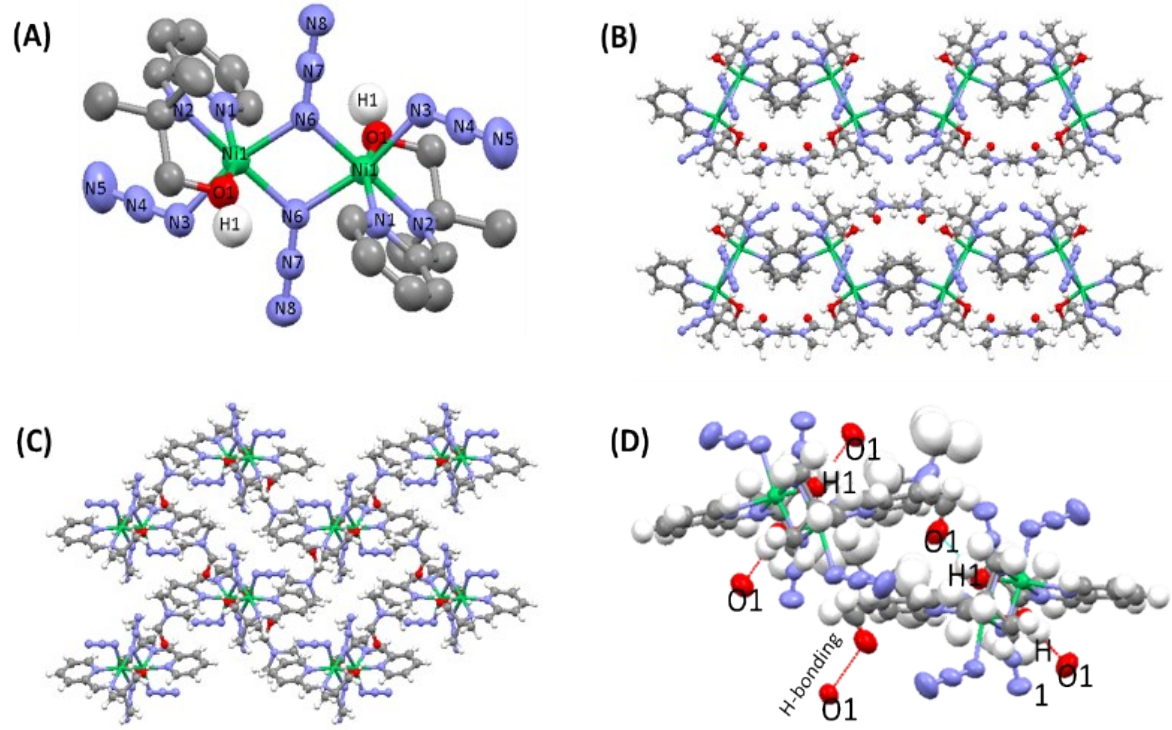


**Fig. S2** (A) Dinuclear symmetrical structure of $Ni^{II}$ (BS-1) (B) Scale like geometry of BS-1

cluster down the c-axis (C) ) Packing of BS-1 cluster down the a-axis (D) Network of H-bonding in BS-1 cluster.

| **Table S1: Selected bond length of the BS-1** | | | |
|---|---|---|---|
| **Bond** | **Length in (Å)** | **Bond** | **Length in (Å)** |
| Ni(1)-O(1) | 2.160(2) | Ni(1)-N(3) | 2.100(2) |
| Ni(1)-N(1) | 2.087(2) | Ni(1)-N(6) | 2.055(2) |
| Ni(1)-N(2) | 2.021(2) | Ni(1)-N(6) | 2.107(2) |
| **Bond length associate to bridging azide of the BS-1** | | | |
| **Bond** | **Length in (Å)** | **Bond** | **Length in (Å)** |
| Ni(1)-N(6) | 2.055(2) | N(6)-N(7) | 1.201(3) |
| Ni(1)-N(6) | 2.107(2) | N(7)-N(8) | 1.140(4) |
| **Bond length associate to terminal azide of the BS-1** | | | |
| **Bond** | | **Length in (Å)** | |
| Ni(1)-N(3) | | 2.100(2) | |
| N(3)-N(4) | | 1.155(4) | |
| N(4)-N(5) | | 1.167(5) | |
| **Selected bond angles of the BS-1** | | | |
| **Bond angle** | **In (°)** | **Bond angle** | **In(°)** |
| N(3)-Ni(1)-N(1) | 91.4(1) | N(6)-Ni(1)-N(1) | 102.2(1) |
| N(3)-Ni(1)-N(2) | 91.5(1) | N(6)-Ni(1)-N(2) | 177.93(9) |
| N(3)-Ni(1)-N(6) | 90.1(1) | N(6)-Ni(1)-N(3) | 167.1(1) |
| N(3)-Ni(1)-O(1) | 88.35(9) | N(6)-Ni(1)-O(1) | 101.12(8) |
| **Bond angles associate with bridging and terminal azide of the BS-1:** | | | |
| **Bond** | **Bond angle in (°)** | **Bond** | **Bond angle in(°)** |
| N(6)-Ni(1)-N(6) | 77.62(9) | Ni(1)-N(3)-N(4) | 120.6(2) |
| Ni(1)-N(6)-N(7) | 125.3(2) | Ni(1)-N(6)-Ni(1) | 102.4(1) |
| **Bond lengths associate with Hydrogen bonding in BS-1:** | | | |
| **Bond** | | **Length in (Å)** | |
| O(2)-H(1) | | 1.801 | |

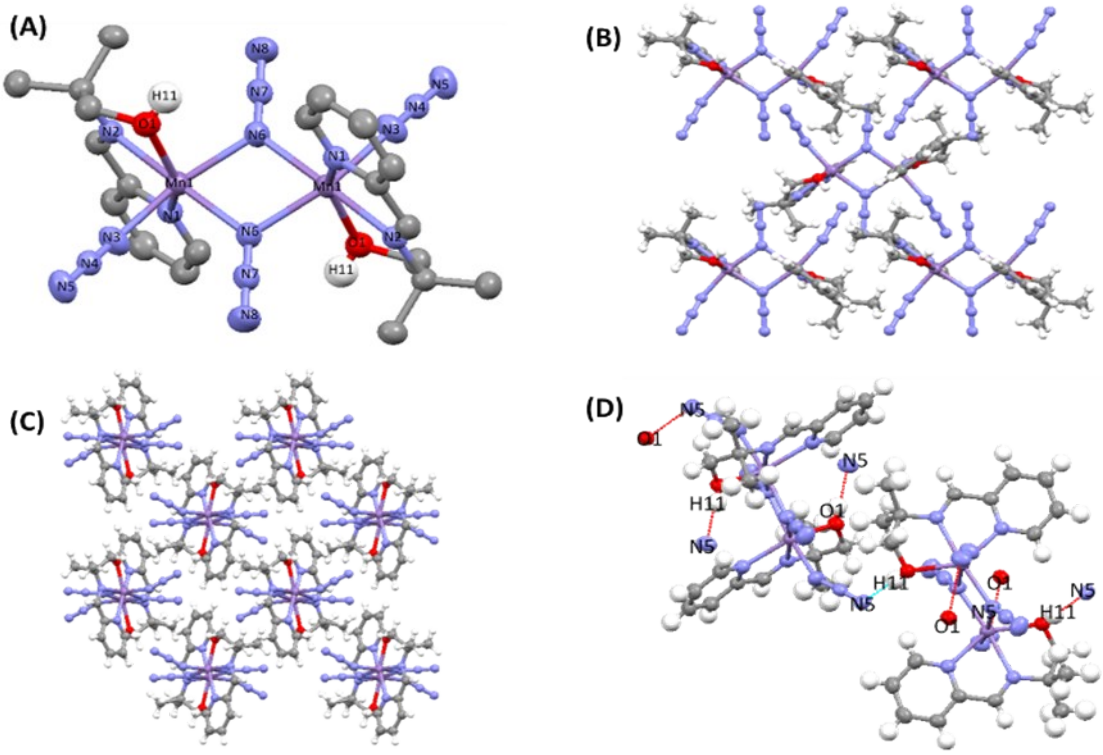


**Fig. S3** (A) Dinuclear symmetrical structure of $Mn^{II}$ (BS-2) (B) Packing of BS-2 cluster down the c-axis (C) Floral geometry BS-2 cluster down the a-axis (D) Network of H-bonding in BS-2 cluster.

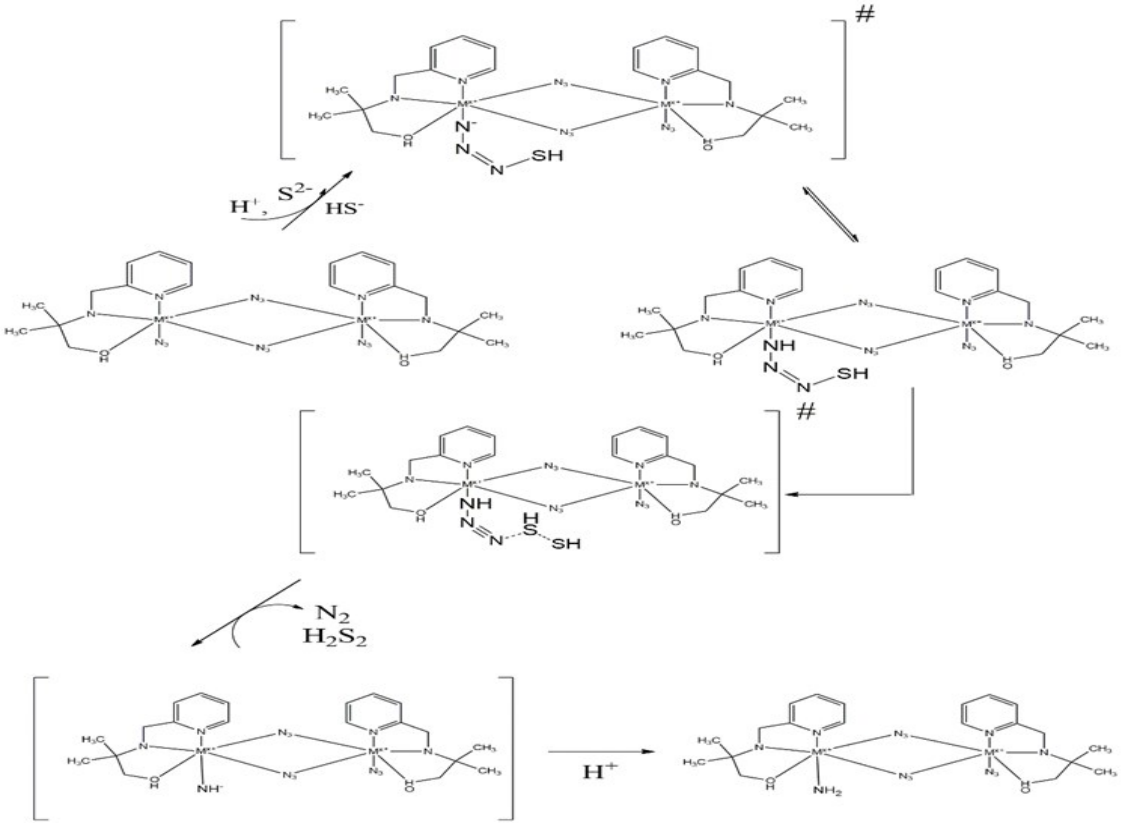

**Scheme S2** Sulphide mediated reduction scheme of azide centre

| **Table S2: Selected bond length of BS-2:** | | | |
|---|---|---|---|
| **Bond** | **Length in (Å)** | **Bond** | **Length in (Å)** |
| Mn(1)-O(1) | 2.240(1) | Mn(1)-N(3) | 2.157(2) |
| Mn(1)-N(1) | 2.284(1) | Mn(1)-N(6) | 2.216(1) |
| Mn(1)-N(2) | 2.265(1) | Mn(1)-N(6) | 2.210(1) |
| **Bond length associate to bridging azide of BS-2:** | | | |
| **Bond** | **Length in (Å)** | **Bond** | **Length in (Å)** |
| Mn(1)-N(6) | 2.216(1) | N(6)-N(7) | 1.177(2) |
| Mn(1)-N(6) | 2.210(1) | N(7)-N(8) | 1.161(2) |
| **Bond length associate to terminal azide of BS-2** | | | |
| **Bond** | | **Length in (Å)** | |
| Mn(1)-N(3) | | 2.157(2) | |
| N(3)-N(4) | | 1.159(2) | |
| N(4)-N(5) | | 1.173(2) | |
| **Selected bond angles of BS-2** | | | |
| **Bond angle** | **In (°)** | **Bond angle** | **In(°)** |
| N(3)-Mn(1)-N(1) | 90.75(5) | N(6)-Mn(1)-N(1) | 113.80(5) |
| N(3)-Mn(1)-N(2) | 92.25(5) | N(6)-Mn(1)-N(2) | 172.49(5) |
| N(3)-Mn(1)-N(6) | 166.71(6) | N(6)-Mn-(1)-N(3) | 91.17(6) |
| N(3)-Mn(1)-O(1) | 91.03(5) | N(6)-Mn(1)-O(1) | 113.80(5) |
| **Bond angles associate with bridging and terminal azide of BS-2:** | | | |
| **Bond angle** | **In (°)** | **Bond angle** | **In (°)** |
| N(6)-Mn(1)-N(6) | 76.42(5) | Mn(1)-N(3)-N(4) | 150.4(1) |
| Mn(1)-N(6)-N(7) | 126.9(1) | Mn(1)-N(6)-Mn(1) | 103.58(6) |
| **Bond lengths associate with Hydrogen bonding in Complex BS-2** | | | |
| **Bond** | | **Length in (Å)** | |
| N(5)-O(1) | | 2.795 | |
| N(5)-H(11) | | 1.988 | |

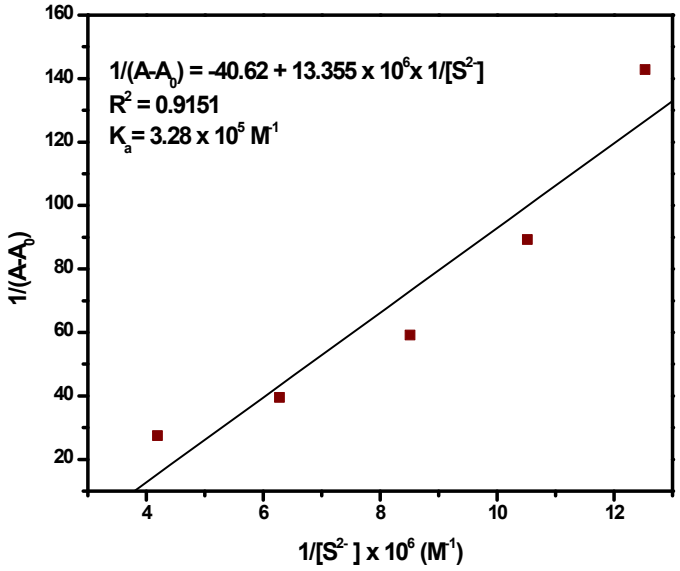


**Fig. S4** Benesi–Hildebrand (B-H) plot for absorbance of $S^{2-}$ with BS-1 for the association constant determination

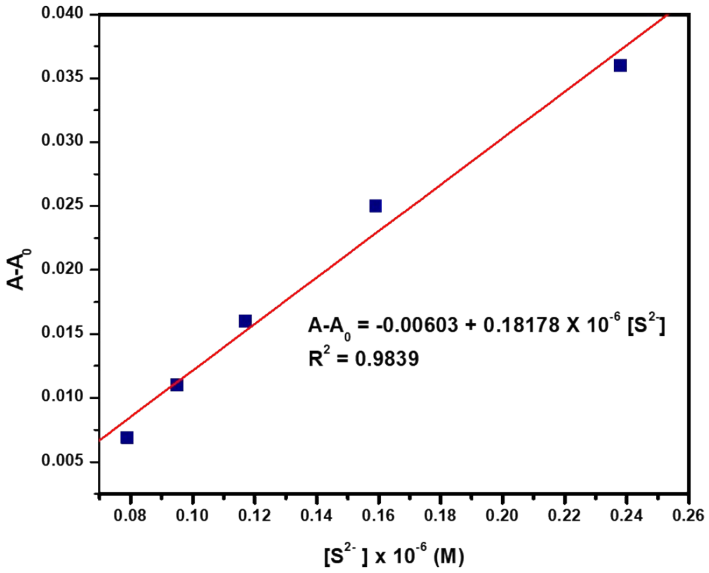


**Fig. S5** Change of absorbance as the function of the concentration of S2- for the calculation of LOD of the complex BS-1 towards $S^{2-}$

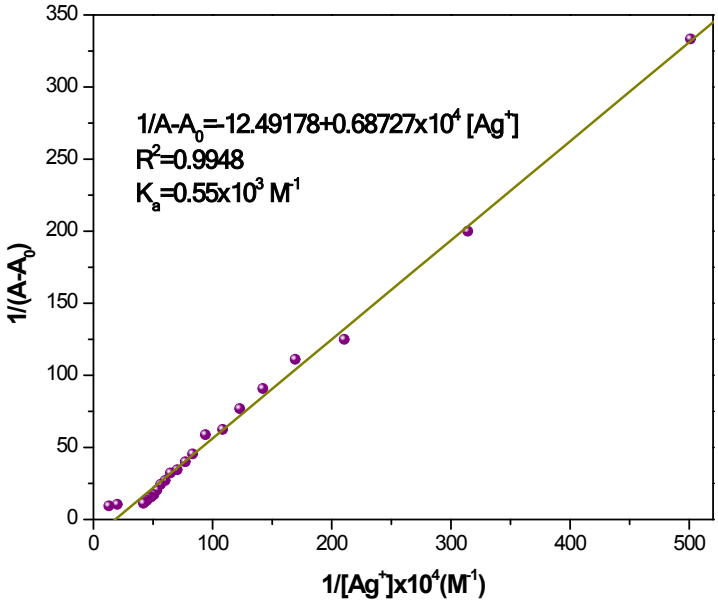


**Fig. S6** Benesi–Hildebrand (B-H) plot for absorbance of $Ag^{+-}$ with BS-1 for the constant association determination

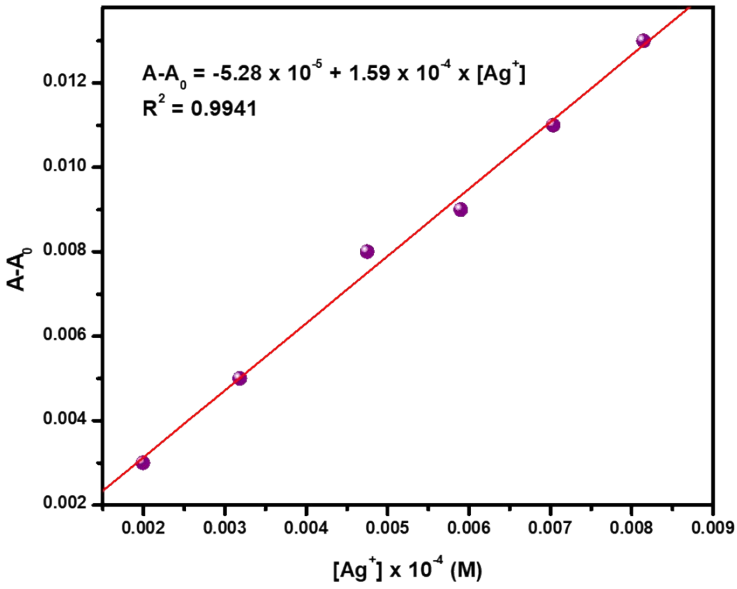


**Fig. S7** Change of absorbance as the function of the concentration of $Ag^{+}$ for the calculation of LOD of the complex BS-1 towards $Ag^{+}$.

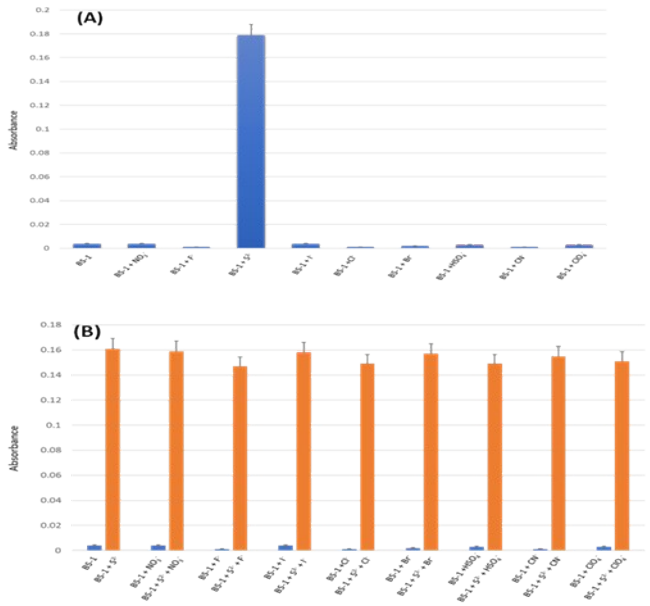


**Fig. S8** (A) Comparative study of BS-1 with different anions in aqueous phase (B) Interference study of BS-1 with different anions in the aqueous phase

In continuation, the selectivity of **BS-1** for other cations apart from $Ag^{+}$ was also investigated for the detection of the toxic analyte from real field samples.

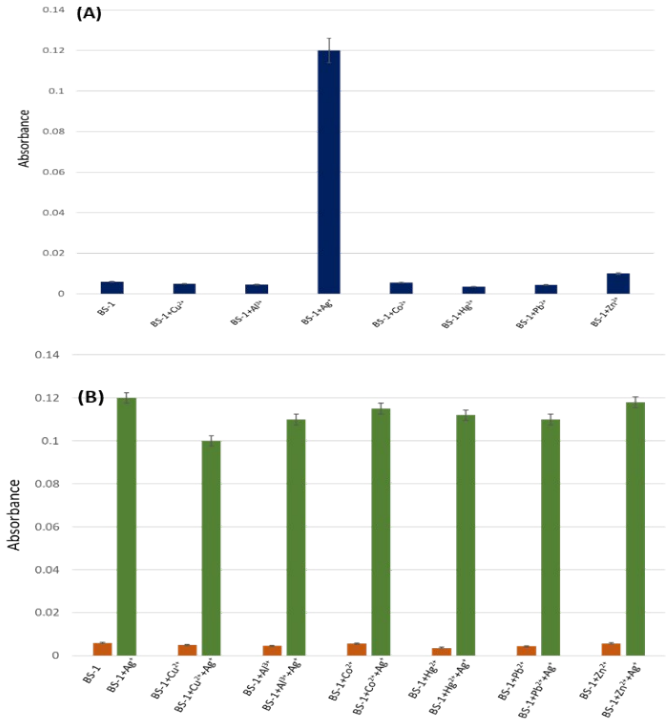


**Fig.S9** (A) Comparative study of BS-1 in DMSO medium with different cations in organo-aqueous phase (B) Interference study of BS-1 with different cations in organo-aqueous phase

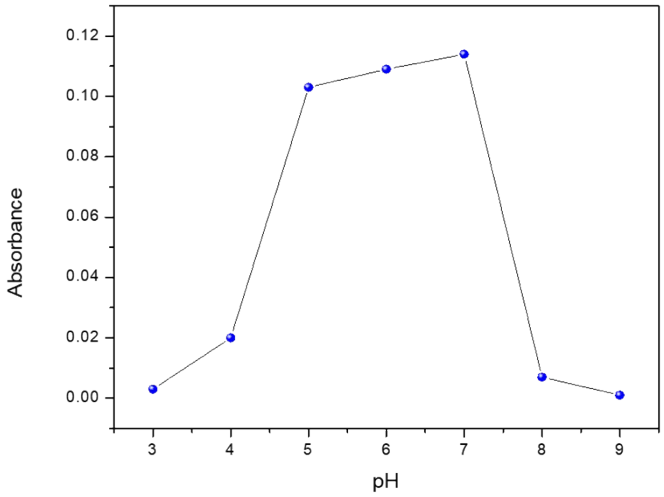


**Fig. S10** Effects of absorbance values of BS-1 with S2- at different pH.

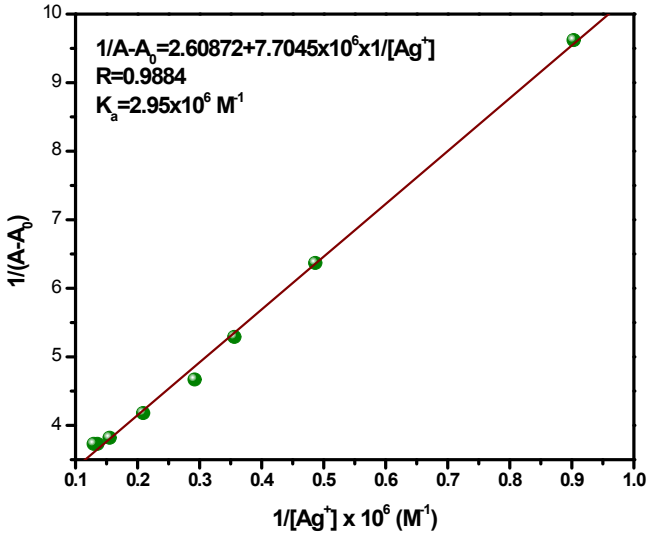


**Fig. S11** Benesi–Hildebrand (B-H) plot for absorbance of $Ag^{+}$ with BS-2 for the association constant determination.

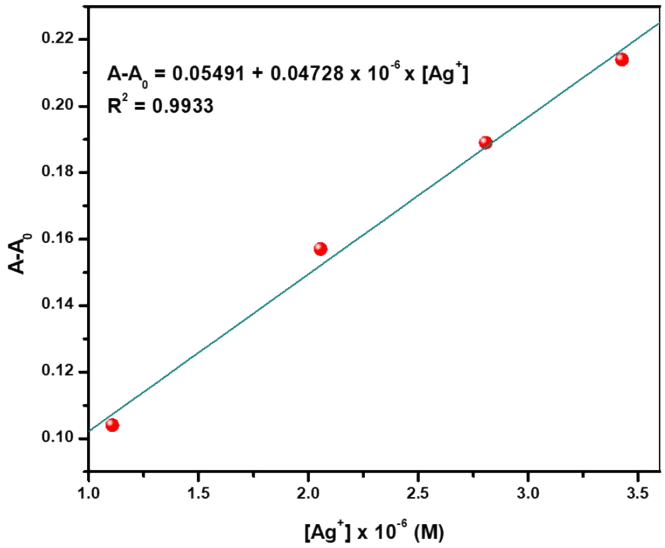


**Fig. S12** change of absorbance as the function of the concentration of $Ag^{+}$ for the calculation of LOD of the complex BS-2 towards$Ag^{+}$

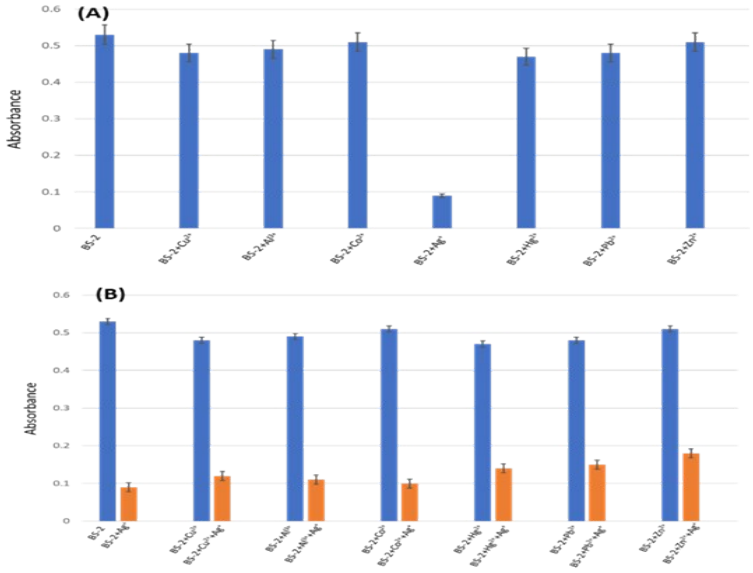


**Fig. S13** (A) Comparative study of **BS-2** with different cations in organo-aqueous phase (B) Interference study of BS-2 with different cations in organo-aqueous phase

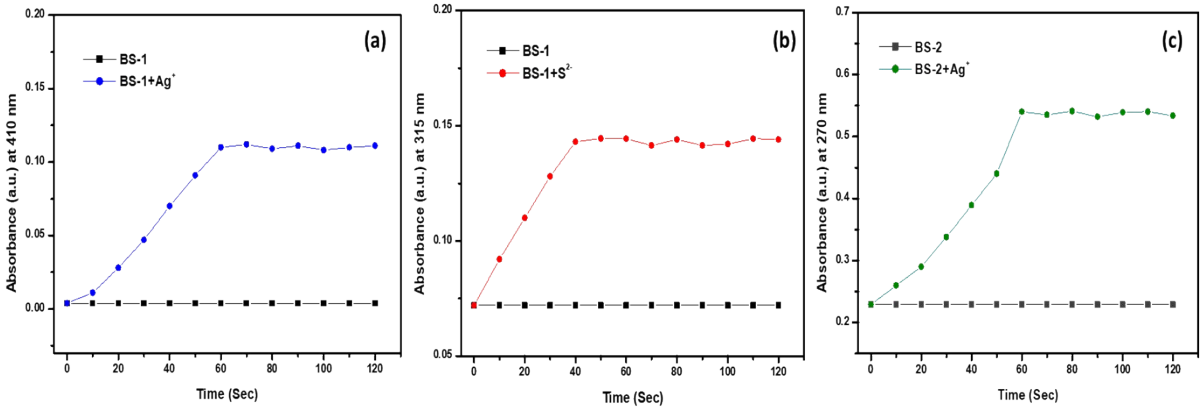


**Fig. S14** Responding time of BS-1 & BS-2 with targeted analytes. (a) Absorbance intensity changes of BS-1 at 410 nm with concurrent addition of $Ag^{+}$ (b) Absorbance intensity changes of BS-1 at 315 nm on gradual addition of $S^{2-}$ (c) Absorbance value at 270 nm changes of BS-2 with addition of $Ag^{+}$

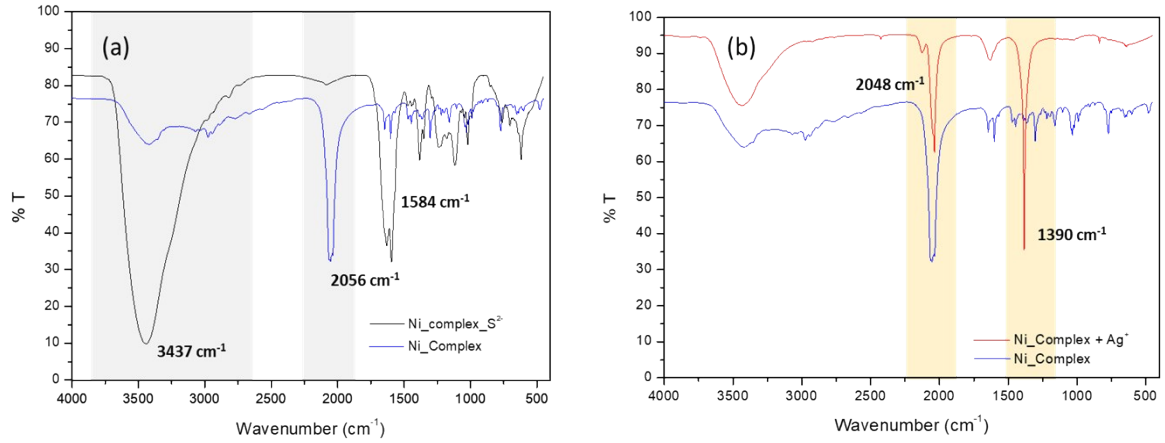


**Fig. S15**(a) FT-IR plot of BS-1 after interaction with $S^{2-}$ (b) FT-IR plot of BS-1 after interaction with $Ag^{+}$

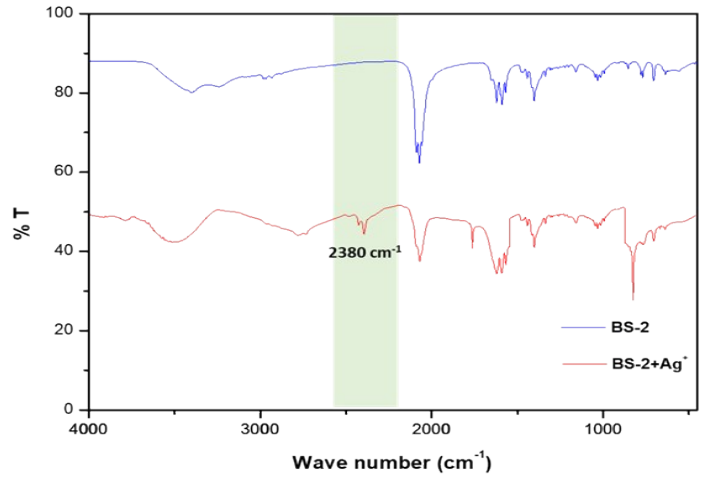


**Fig. S16** Ag-N stretching frequency at 2380 $cm^{-1}$ after interaction of BS-2 with $Ag^{+}$

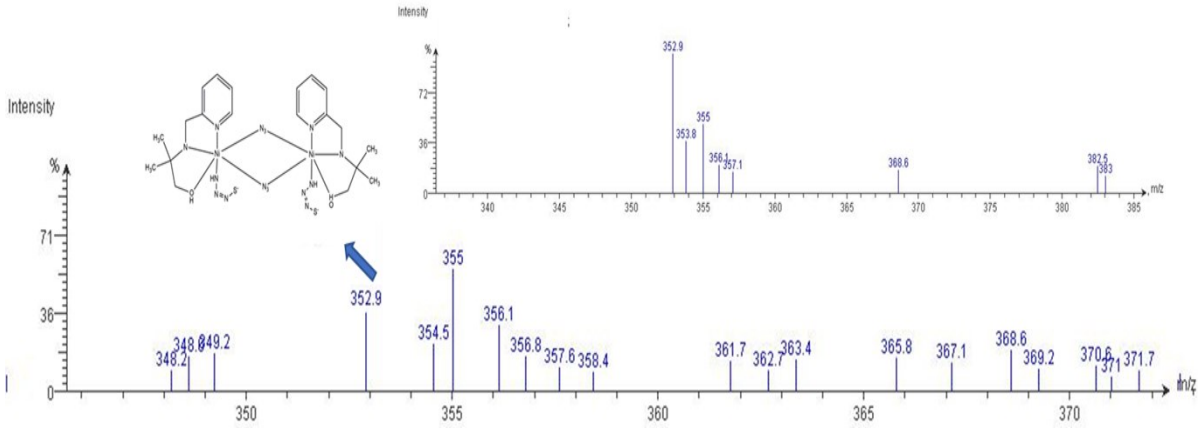


**Fig. S17** ESI-MS data of **BS-1**---$S^{2-}$ adduct through an intermediate { [-NH-N=N-SH]$^{\#}$} formation

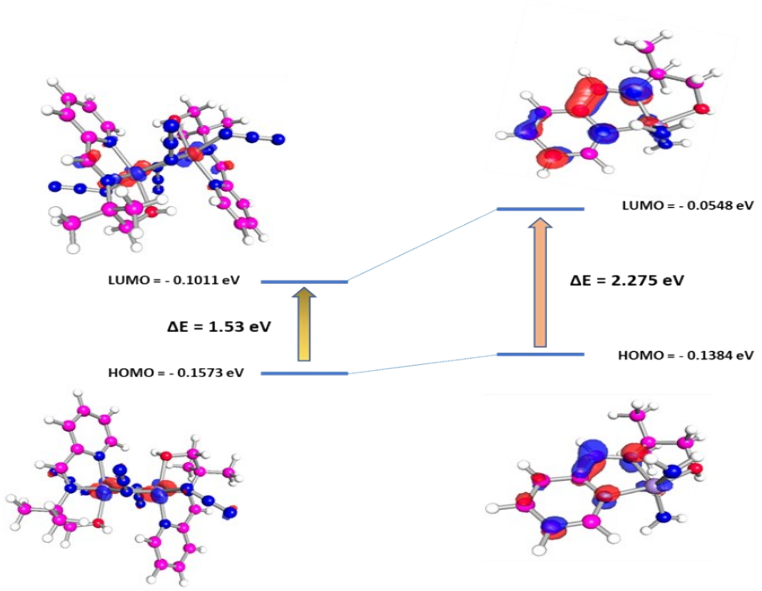


**Fig. S18** Geometry Optimised structure and HOMO-LUMO band gap of monomeric unit of chemosensor BS-2

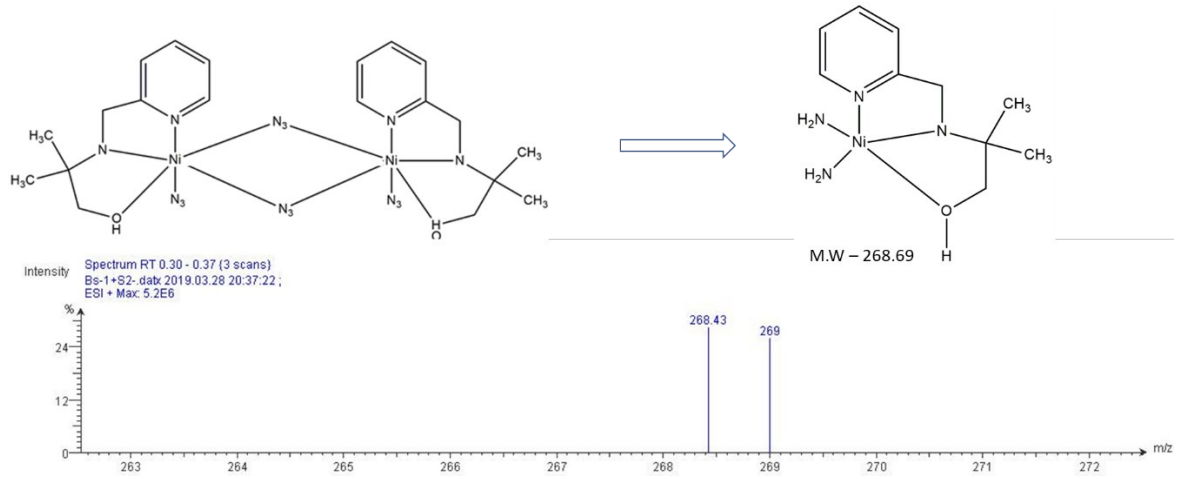


**Fig. S19** ESI-MS data of BS-1-monomeric unit after reduction by $S^{2-}$

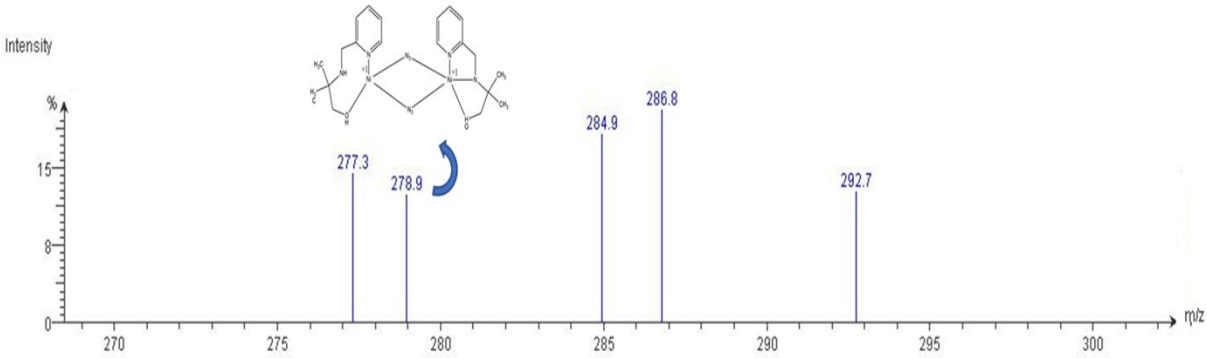


**Fig. S20** ESI-MS data of BS-1---$Ag^{+}$ adduct through Ag-N bond formation

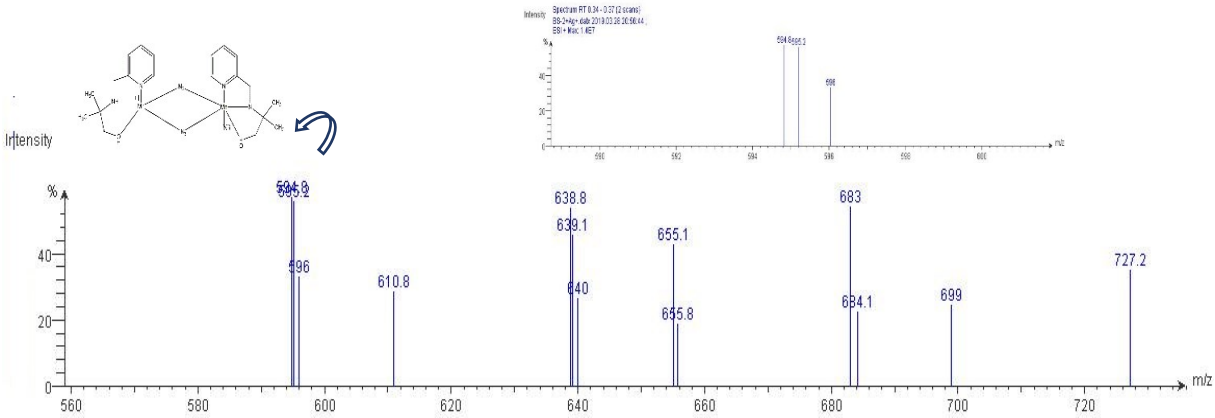


**Fig. S21** ESI-MS data of **BS-2**---$Ag^{+}$ adduct through Ag-N bond formation